SYNTHESIS AND CHARACTERIZATION OF GRAPHENE BASED BARIUM TITANATE PIEZO-NANO COMPOSITE MATERIAL

by

Ashok Kumar Pasumarthi

A Thesis Submitted in Partial Fulfillment of the Requirements for the Degree in Masters in Engineering Technology

Middle Tennessee State University

December 2019

Dissertation Committee:

Dr. Vishwas Bedekar, Chair

Dr. Suman Neupane

Dr. Walter Boles

ABSTRACT

Applications in various fields of technology like microelectromechanical systems (MEMS), Energy Harvesting, sensing and energy storage, etc., made graphene a unique material of all the carbon allotropes. Barium titanate ($BaTiO_3$) on the other hand is a lead-free piezoelectric ceramic material, which has good applications in the fields of medicine, energy harvesting, sensing, and actuator applications. Mono-layer graphene and its extensive electronic properties make it a prominent substrate material for many applications. In this thesis, we would present the detailed approach of synthesis of a few-layer graphene on a copper template using chemical vapor deposition (CVD) technique at atmospheric pressure. Raman spectroscopy is used for the characterization of a few-layer pristine graphene. Thermo-gravimetric analysis is used to measure the yield of graphene on copper foil. Ultrasonication coating of $BaTiO_3$ on few-layer graphene followed by the characterization of the resultant graphene and barium titanate composite material using X-ray photoelectron spectroscopy, X-ray diffraction, scanning electron microscopy and Energy dispersive X-ray spectroscopy will confirm the presence of elements and phase transformation.

TABLE OF CONTENTS

List of Figures

List of Tables

CHAPTER I: INTRODUCTION

Graphene is an atomic thick two-dimensional allotrope of carbon. It was discovered by KS Novoselov and AK Geim by mechanical exfoliation of pyrolytic graphite [1]. In this case, graphene, which was termed as few-layer graphene (FLG) is 10μm in size and stable at room temperature [1, 2]. Sp^2 hybridization of carbon atoms in graphene is responsible for its notable electrical properties and stability in lattice structures. The σ-band in sp^2 hybridization accounts for stability while the π-band results for electronic properties [3]. Scanning tunneling microscopy image of single-layer graphene showing the honey-cube formation of carbon atoms at 1nm magnification is shown in the following figure [4].

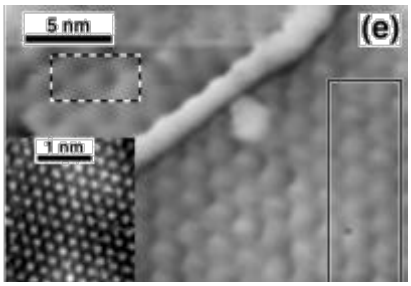

Figure 1. STM image of Graphene at 1nm

Reprinted with permission from (https://doi.org/10.1021/jp040650f). Copyright (2004) American Chemical Society.

Graphene is a blend of semi-conductor and metal showing properties of soft matter. Applying the electric field or Magnetic field or adding impurities by doping or increasing the number of layers can easily modify the electronic properties of the graphene [3]. Nano-composites and Nano-ceramics are the extensive fields of

research in the past few years due to their diversified fields of applications. The surface area of the substrate (filler material) plays a vital role in the uniform distribution of adsorbent material [4].

The specific surface area of graphene is 3523 m^2/g [5]. Graphene is notable for electron-hole degeneracy, almost-zero effective mass, ultrahigh mobility, and long mean free path [6]. Hence the combined physical and electrical properties makes graphene a good substrate material at the Nano-scale.

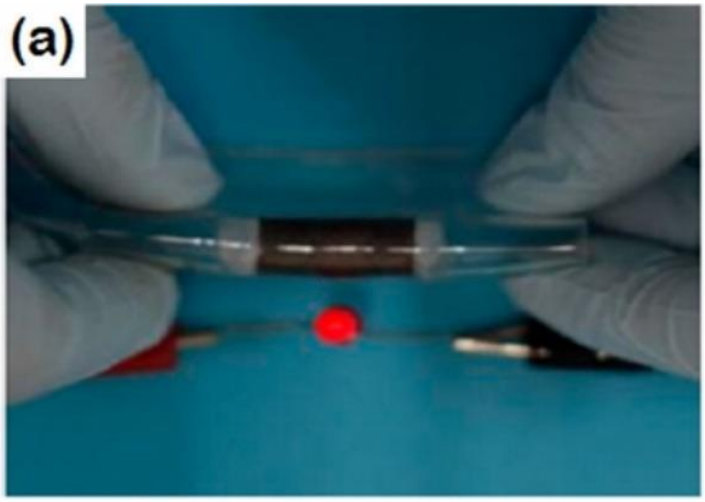

Figure 2. Optical image of Graphe flexible electrode

Reprinted with permission from (https://doi.org/10.1021/jz400005k). Copyright (2013) American Chemical Society.

Graphene has great potential in the fields of optoelectronics like OLEDs and micro-electronic devices like field effect transistors and energy harvesting devices like electrochemical capacitors, hybrid solar-cells [7-10]. The optical image of the graphene electrode flexible electrode is shown in above figure [10].

Wireless Strain Sensors

Graphene produced by using of gravure printing method is coupled with reading Antenna as shown in the figure 3. According to Faraday's law sinusoidal AC, voltage signal passing along the reading antenna produces a magnetic field. As a result, there will be inductive coupling between the reading antenna and the printed graphene coil. The changes in the graphene coil characteristics can be wirelessly detected based on the change in the complex impedance of the reading antenna. A schematic diagram is shown in the figure. WSS is mainly used in detecting structural changes in the human body [11].

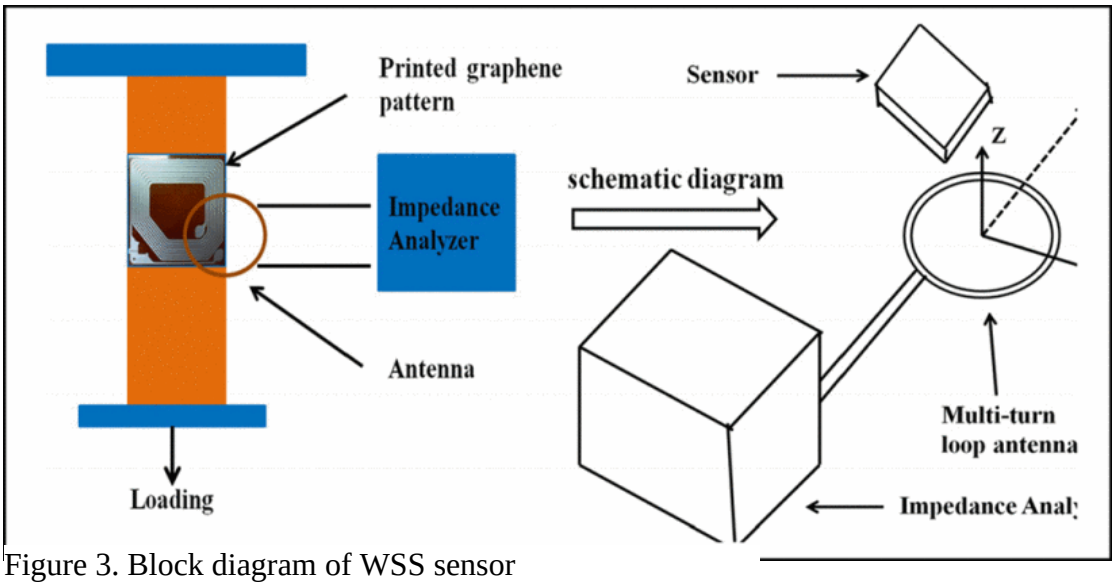

Figure 3. Block diagram of WSS sensor

Thermoelectric Generator (TEG)

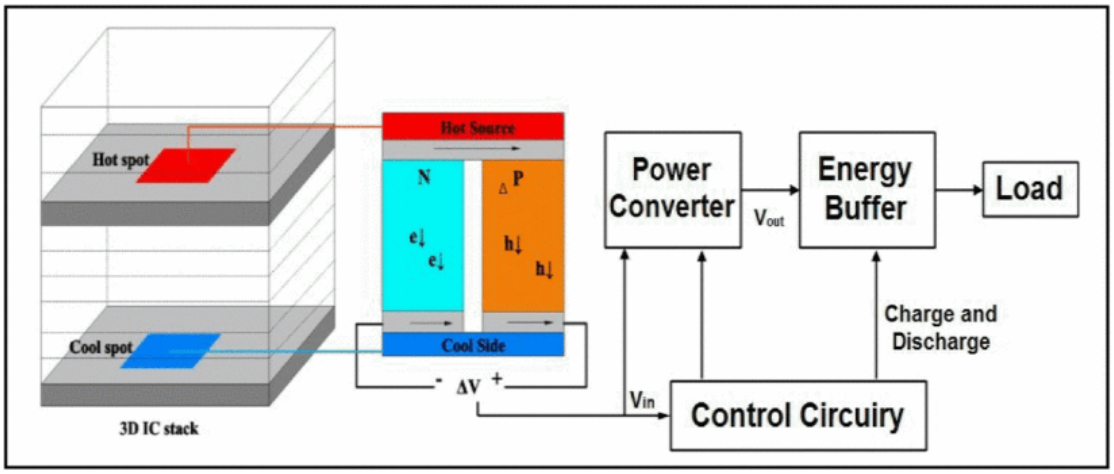

Figure 4. Block diagram of Thermo-electric Generator

According to See beck effect voltage is produce when there is a temperature difference in thermocouples. The heat generated in the 3D integrated circuits (IC) can be utilized to generate power and can be utilized within the IC**,** this reduces heat and power consumption of the whole IC itself. Since graphene is a 2D material with high thermal conductivity and occupies less space plays a vital role in TE devices. Graphene P and N-type layers are fabricated between silica layers. The electron and hole moments in the graphene layers caused due to the temperature difference will produce a potential difference. Resultant power can be converted and stored in an energy buffer, like a capacitor and can be used when required [12].

Graphene Solar cells

Photovoltaic cells are carbon emission-free energy harvesting devices. But when compared to other large scale energy harvesters like wind turbines the output is very low. To improve efficiency and flexibility is on-going research. Graphene is a good conductor of electricity with high transmittance and low reflectiveness can improve efficiency. P doped Graphene quantum dots and N doped silica can be fabricated to form a Schottky junction and used a photovoltaic cell [13].

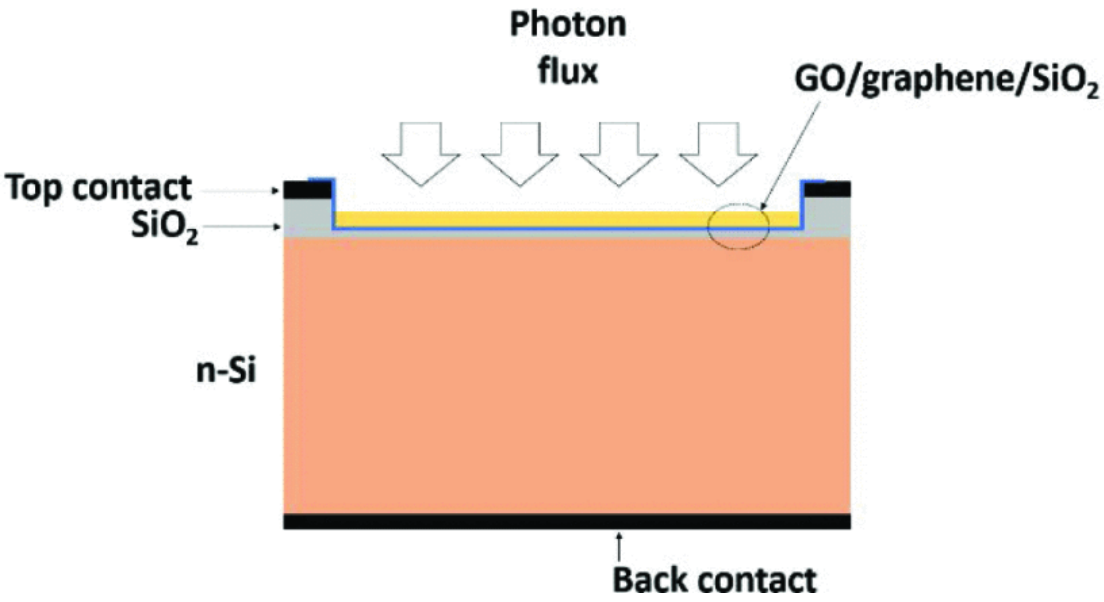

Figure 5. Block diagram of Graphene Solar cell

Graphene Industries

1. Haydale produces stronger, lighter and fuel-efficient automobile components. It provides functionalized graphene coatings for air crafts which increases the electrical conductivity due to thunder strikes by 600%. It makes inexpensive medical implants for diabetes patients and graphene-based inks for biosensors [14].
2. Graphena Produces and sells graphene precursors and pristine graphene samples which can be used for optimization and conducting research. We can customize graphene layers by special orders [15].
3. Talga is a graphite mining company in Sweden it produces graphene products used for coatings, batteries, and concrete and epoxy composites [16].

Barium Titanate ($BaTiO_3$)

Barium Titanate ($BaTiO_3$) functional material is widely used in sensing, actuating and energy harvesting applications. $BaTiO_3$ is an ABO_3 perovskite-type structural material. It has good dielectric, piezoelectric and ferroelectric properties [17-19]. We have chosen $BaTiO_3$ as our functional material for graphene as it is lead-free piezoelectric nano-ceramic material [18-20]. Also, of all the lead-free materials $BaTiO_3$ has shown high piezo-electric properties close to the lead-based PZT materials [17-19]. Zarkoob, H., et al [20] produced barium titanate bio ceramic sensor material for biomedical applications using nano phase hydroxyapatite coating. Potential in the fields of medicine and engineering has compelled us to pick Barium Titanate as a functional material for graphene composites.

CHAPTER II: LITERATURE REVIEW

Novoselov, K. S., et al [1] have discovered the existence of various 2D crystals by micromechanical cleavage method and graphene is one of them, which is produced from pristine graphite. Graphene produced by this method is highly contaminated with adhesive, but the graphene is pristine and monolayer, even though this method is cheap and easy, transferring of graphene to any other substrate is hard and cause defects in the graphene layer. Berger, C et al [21], produced graphene using the epitaxial growth method by desorption of silica from silicon carbide (SiC) using an ultra-high vacuum. This method eliminates the transfer process as it is produced by the consumption of template (SiC), but SiC is not a good template in the case of piezoelectric applications. Silicon carbide is an expensive precursor and the amount of graphene is limited to the amount and size of SiC used. Also, this method requires high temperatures from 1250℃ to 1450℃ and ultrahigh vacuum which makes the process more complicated. Sahoo. S et al [22] used high-grade pyrolytic graphite sheets as electrodes and perchloric acid as the electrolyte to produce graphene. Graphite sheets are chemically exfoliated when the voltage is increased, the resultant

graphene is not pristine it is graphene oxide and it involves centrifuging process to separate the graphene from the electrolyte, purity, and yield are low. S. Moshgi et al [23] used sulphuric acid and sodium nitrate to produce graphene oxide from graphite sheets by pulse potential electrode deposition, the process takes days stirring the chemicals to make it homogenous, chemicals used are expensive and a cumbersome process, end products are contaminated with iron and zinc coming from precursors used. Huang et al [24] used electron cyclotron resonance chemical vapor deposition to produce pristine graphene films on copper foil at 600℃. Methane is the precursor and used as radicals in the plasma, the equipment uses microwaves for producing plasma. This technique is very helpful in the industrial-scale production of graphene. This process is expensive and there are hazards of radiation. Dagher et al [25], presented the growth of graphene on Aluminum Nitride (AlN) using propane precursor at a temperature of 1350 to 1450 ℃ on silicon carbide substrate. They have produced AlN on SiC and then used the resultant product as a substrate for CVD of graphene. This technique needs high temperatures and the graphene is contaminated with aluminum nitride and the whole process is expensive, to improve the yield this method has to be conducted at higher temperatures and low pressures. Kim. J et al [26] used forced

convection plasma-enhanced CVD to produce graphene at a lower temperature of 400℃ on Cu substrate. They showed that the quality of graphene increased with the growth time of plasma. This method produces pristine graphene on an industrial scale. The process is expensive and the plasma is the source of radiation and hazardous. Golap Kalita et al [27] used camphor as a precursor and Ni precursor to produce graphene using CVD. The graphene produced is pristine and can be transferred to any other substrate easily for further analysis. But this method needs a double stage furnace because camphor evaporates under 200℃. Juang, Z.-Y et al [28], produced single to few-layer graphene at 900Torr or 1 atmospheric pressure on 30μm thick nickel foil using CVD technique. We repeated the process by using the Cu foil as a substrate at atmospheric pressure and 900℃, the reason for choosing copper substrate it has a lower melting point than nickel and uniform deposition takes place when the substrate is heated close to the melting point. Lee, J et al [29] explained the correlation between the template exposure times to the etching element, which is 5.8% Nitric acid to the graphene growth. But this method is complicated since the variation in concentration of nitric acid or the exposure time could dissolve a copper film of 0.025mm thickness. Also, Nitric acid oxidizes the film which is not desired in

the material characterization. We used hydrochloric acid (HCl) as etchant which did not vary the graphene growth or surface properties of copper.

Table 1. Summary of Graphene synthesis methods

REF	Author	Method	Material and Precursor	Remarks
1	Novoselov	Mechanical exfoliation	Graphite and scotch tape	Contamination of graphene due to the adhesive material
21	Berger.C	Epitaxial growth	Sic and silica wafer	Expensive and Cumbersome process, defective graphene
22	Sahoo, S.	Electrochemical exfoliation	Graphite sheets perchloric acid	Graphene contaminated with Graphite
23	Moshgi	Pulse potential Electro-deposition	Graphite, Sulphuric acid, Sodium Nitrate	Graphene is contaminated with Managed and Iron
24	Huang	Electron Cyclotron resonance CVD	Methane and copper foil	Expensive equipment and Microwave Radiations
25	Dagher	CVD	Propane, Aluminum Nitride, and Silicon Carbide	Expensive Precursor and Graphene is defective and contaminated with AIN
26	Kim J.	Forced Convection Plasma enhanced CVD	Cu foil plasma of carbon radicals	Microwave radiations and parameter controls are complex
27	Golap Kalita	CVD	Camphor and Nickel	Contamination of carbon black
28	Juang	CVD	Nickel and Methane	Higher temperature
29	Lee J	CVD	Copper, Methane and Nitric acid	Thin copper foil can dissolve in Nitric acid

From the summarized table of literature, we choose Cu as our substrate, methane (CH_4) as a precursor. We have conducted this growth at 900℃ at atmospheric pressure. The copper substrates after graphene growth are characterized by Raman spectroscopy.

Castro, E. V., et al [3] examined that electron-hole asymmetry terms have less effect on the electronic properties of bilayer graphene. Xuesong Li, et al [30], measured the mobility of charge carriers in CVD graphene grown on copper as 4050 $cm^2\ V^{-1}\ s^{-1}$ and carrier concentration as $3.2x10^{11}\ cm^{-2}$. Wu, Y., et al [22] built hybrid heterojunction solar cells using transparent conductive graphene. Babichev, A. V.et al [8], compared and analyzed the contact resistance of few and monolayer graphene with different metals. Dong Soo Choi et al [9], fabricated a flexible electrochromic device using three-layer graphene. ALYÖRÜK, M. M. Et al [31], examined that coaxed graphene with asymmetric holes shows good piezoelectric properties than pristine graphene. Brazhe, R. A., [32] et al, measured the piezoelectric modulus of perforated graphene equals to 0.14 pC/N.

By reviewing the literature of various applications, we can conclude graphene has good electron properties and a suitable substrate material for sensing and energy harvesting applications.

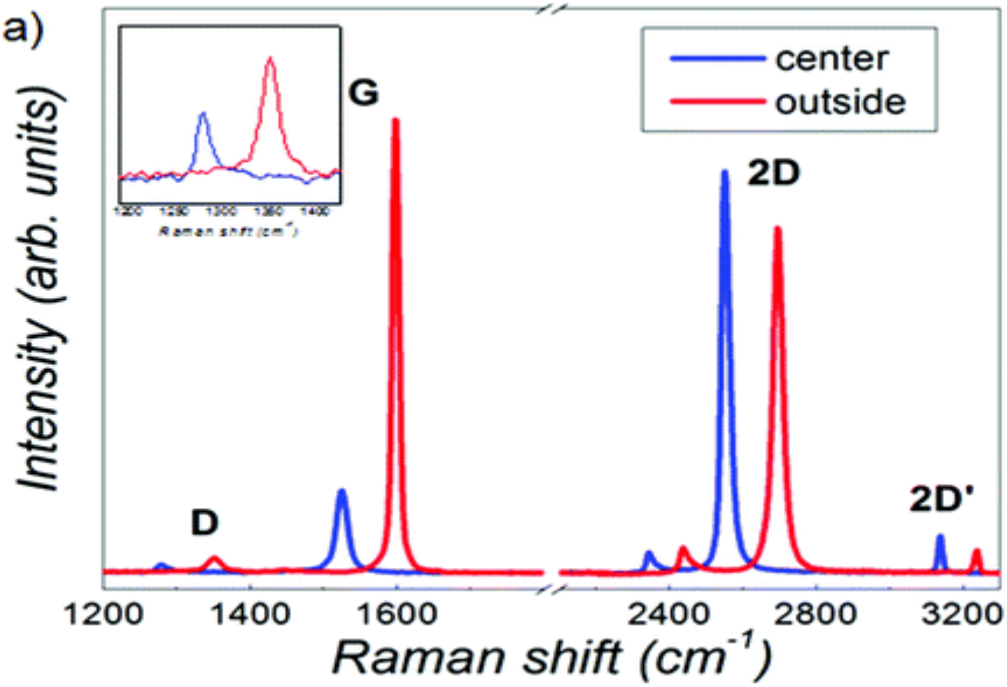

Figure 6. Raman spectra of Graphene

Reprinted (graph) with permission from (https://doi.org/10.1021/nl203359n).

Copyright (2012) American Chemical Society.

Zabel et al [33] have conducted the Raman spectroscopy of graphene. Depending on the purity and number of layers D, G, D' and 2D peaks show up. D peak is responsible for the breathing modules, occurring around 1360 cm^{-1} due to the vibration of sp^2 hybridized atoms. G peak is the Gaussian peak that occurs around 1580 cm^{-1} corresponds to the Bernoulian zone. D' characterizes the graphene showing the presence of Defects occurs b splitting of G peak around 1620 cm^{-1}. Sharp 2D confirms that Graphene as monolayer otherwise it is a few-layer Graphene.

Kumazawa, H. Et al [34] examined that the high dielectric coefficient of $BaTiO_3$ produced by the dip-coating method occurs at 800℃. Dip coating does not guarantee the uniform distribution of barium titanate particles all over the graphene which is a few-layer thick and randomly dispersed all over the copper substrate. In dip-coating the precursor is held by viscous drag and surface tension, which are weak physical forces. Sing M et al [17] synthesized and sintered $BaTiO_3$ using sol-gel and spin-coating techniques. Spin coating is a decent technique to ensure uniform distribution of precursor, but spin-coaters are expensive, substrate flatness of substrate plays a vital role in the spin coating. This technique is not adopted for coating samples which are not flat and powdered samples. Jelena Vukmirović et al [18] characterized and compared inkjet printing and spin-coating of $BaTiO_3$ thin films. The inkjet printing process is sophisticated and expensive, it is better than conventional spin-coating technique. Hu, S., Luo [19] examined the effect of sintering temperatures on the piezoelectric coefficient of $BaTiO_3$ and shown that at1350℃ $BaTiO_3$ has a d_{33} value of 420 pC/N.

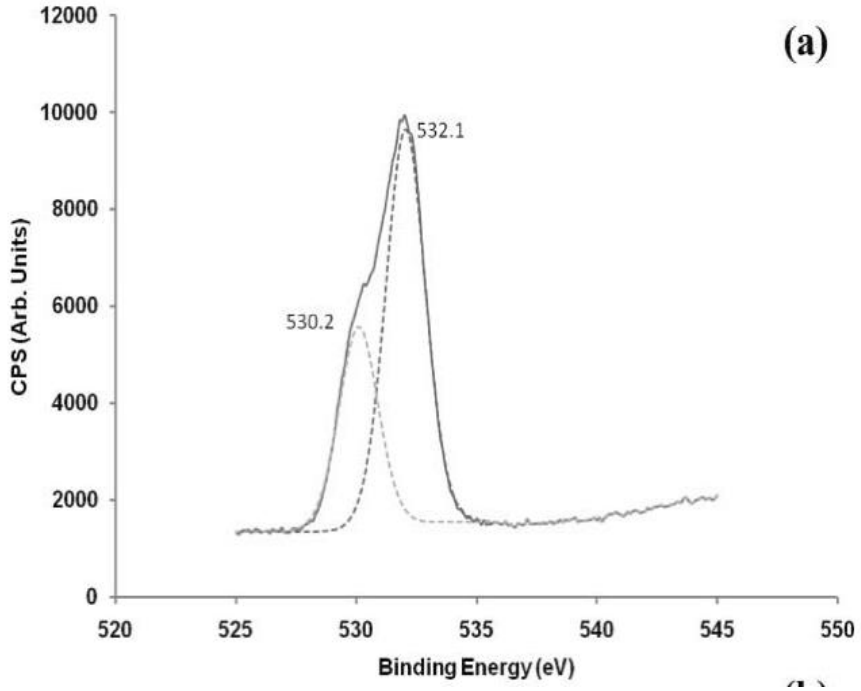

Figure 7. XPS showing Binding Energy peaks of oxygen in BaTiO3

Bedekar.V et al [35-36] have presented the coating of barium titanate on multiwall carbon nanotubes using a cost-effective ultrasonication technique. Ultrasonication ensures the thorough mixing of precursor and the graphene, it also improves the adhesiveness of the substrate. It is a cost-effective coating-method when compared to any other method we have discussed earlier in the literature. We used the same coating method to coat few-layer graphene with $BaTiO_3$ since graphene and carbon nanotubes are both sp2 hybridized carbon allotropes. We sintered the samples at 700℃ and 900℃ characterized using X-ray photoelectron spectroscopy.

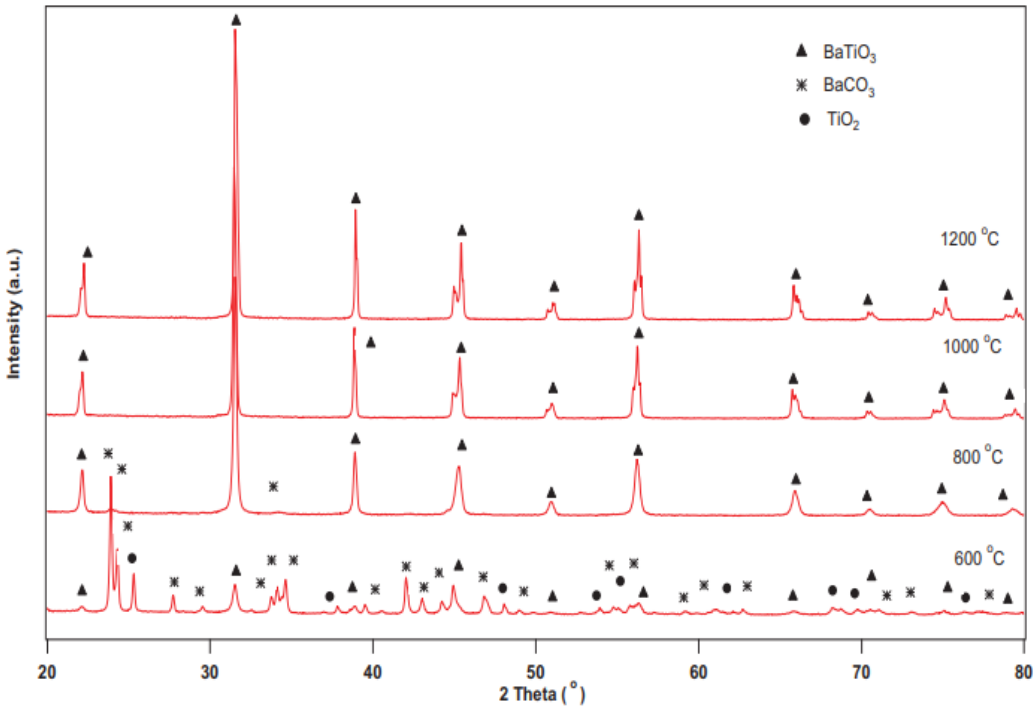

Figure 8 XRD analysis of BaTiO3 at various temperatures

Reprinted with permission from AIP conference proceedings.

According to Zali et al [37], calcination temperatures and time play a vital role in the sintering of barium titanate. XRD peaks of barium titanate sintered at 600℃ to 1200℃ are shown in the chart. Above 800℃ we can see the XRD analysis show sharp and narrow peaks, saying that the resultant barium titanate has reached its crystallinity. At 600℃ we see unreacted barium carbonate and titanium oxide, which means the calcination temperature of 600℃ and growth time of 2 hours cannot result in the BaTiO3. But increasing the calcination temperature above 1000℃ has shown the sharp peak of Barium titanate around 32º of 2-theta value. Also, by sintering at elevated temperatures $BaCO_3$ and titanium oxide peaks disappear.

CHAPTER III: OBJECTIVES OF RESEARCH

In order to achieve barium titanate coated graphene for energy harvesting and sensing applications following objectives of research have been identified and demonstrated in this thesis.

- Synthesis of mono/few-layer graphene using chemical vapor deposition technique on copper substrate
- Synthesis of sintered barium titanate layer over graphene using precursor and ultrasonication technique
- Materials characterization of the synthesized nanostructure to confirm phase transformation and bonding of elements.

CHAPTER IV: GRAPHENE SYNTHESIZATION TECHNIQUES

Depending on the quality and the quantity of the graphene several growth techniques are adapted. Of all the techniques Mechanical exfoliation, Chemical exfoliation, Epitaxial growth, and thermal chemical vapor deposition are widely used.

Mechanical Exfoliation

Scotch tape is used to exfoliate the topmost layers of pyrolytic graphite. The graphene produced with this technique is a few layers thick and pristine, which can be later transferred on to any substrate for further analysis. This resultant graphene is useful for research but bulk-scale production is not possible and the graphene is contaminated with adhesive material of scotch tape. Geim and Novelsolv used this method in their early-stage analysis of Graphene. [1, 31]

Chemical Exfoliation

This technique is utilized in the production of Graphene oxide and reduced graphene oxides. Initially, Graphite is dissolved in strong oxidizing agents like acids. Then water is added to make a hydrophilic solution. Water increases the D-spacing of graphitic layers and exfoliates the graphene oxide layers from graphitic oxide. The resulting graphene oxide layers are treated with reducing agents like hydrazine and dimethyl hydrazine to obtain reduced graphene oxide sheets. These reduced graphene oxide sheets are not pristine graphene. They have surface defects which can later be mitigated by annealing [38-39].

Epitaxial Growth

Silicon carbide (SiC) is used as a substrate and precursor in this method. SiC is heated to an elevated temperature of 1200℃ to 1600℃ under vacuum. As a result, silicon is evaporated from the surface leaving behind carbon. The resulting carbon compound is pristine and large area graphene. This technique requires large amounts of SiC which is expensive also higher temperatures are difficult to handle [21, 38].

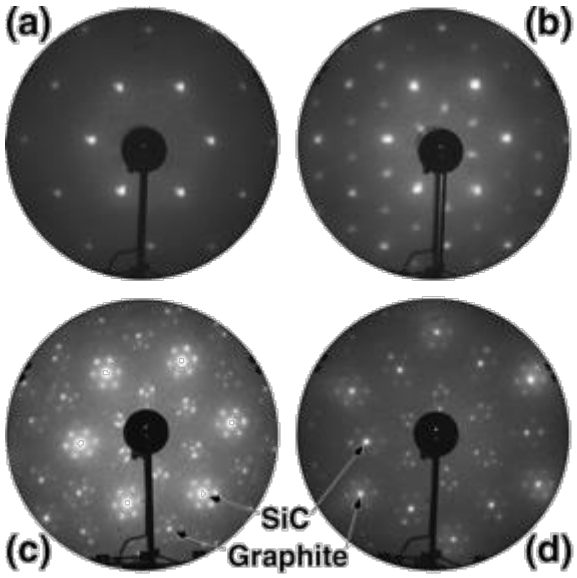

Figure 9. LEED patterns of Graphite on SiC

Chemical vapor Deposition

Chemical vapor deposition (CVD) is a self-limiting and single-step process. Copper (Cu) and nickel (Ni) are widely used metal substrates, methane is the precursor and source of carbon. Hydrogen and copper are catalysts. The copper substrate, as well as catalyst, is responsible for the dehydrogenization of methane and deposition of carbon at high temperatures. Copper or nickel are preheated to an elevated temperature close to their melting points in an inert medium then methane is passed over the substrate. Ideally, the obtained graphene is a monolayer, but there are surface defects of Graphene. This technique results in the large area growth of pristine graphene flakes [24-25, 40]. This method is highly adopted for producing graphene on a large scale because of the high quality of the graphene obtained and lower costs.

Theoretically, the process is self-limiting because when there are no grounds of copper available for deposition then the dehydrogenization stops and results only mono-layer graphene. But practically few-layer graphene is obtained depending on the other parameters like pressure and purity of the substrates used. The graphene obtained by this process can easily be transferred on to any other substrate by using the polymethylmethacrylate (PMMA) since copper is soluble in organic solvents. The abundance and low cost of precursors and catalysts make CVD a promising technique in the production of high-quality techniques [9, 38].

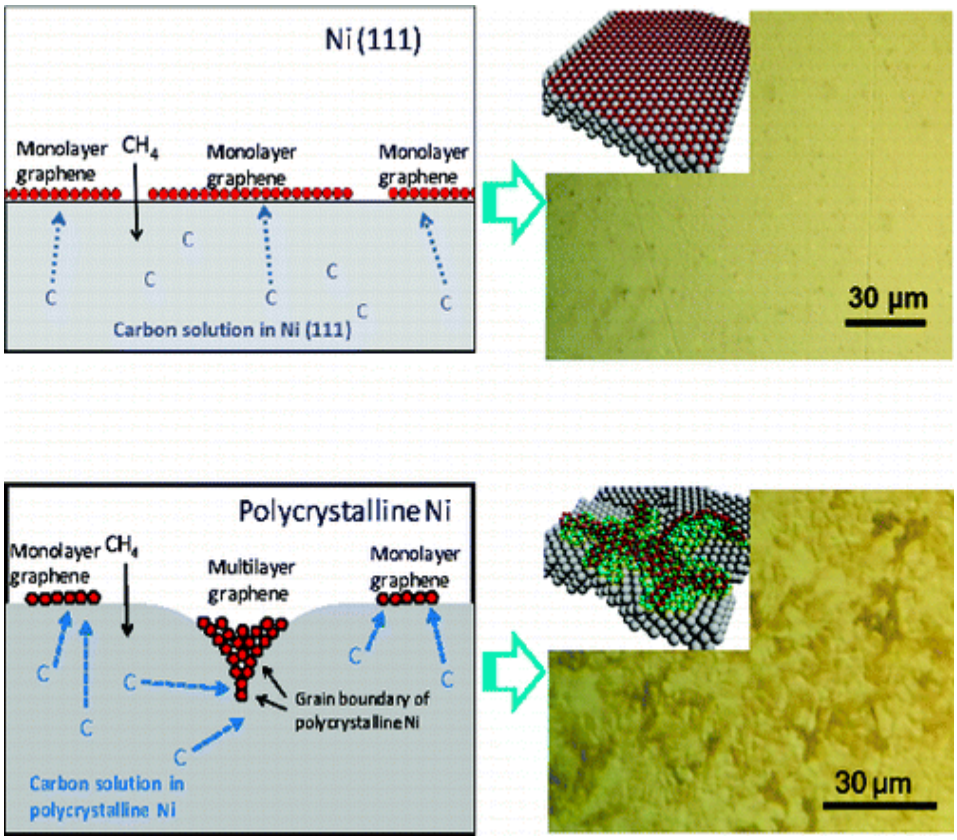

Figure 10. Graphene growth on Ni foil using CVD

CHAPTER V: MATERIAL CHARACTERIZATION TECHNIQUES

Raman Spectroscopy

When light is incident on any solids, liquid or gas medium it gets absorbed, emitted, transmitted, scattered and reflected. Scattering of light is caused due to the interaction of photons of light and medium. Scattering of light helps in the study of *"internal structure and motion of matter on both macroscopic and microscopic scales"* in scattering energy of light is changed resulting in the change in wavelength, whose units are cm^{-1} or wavenumber, this phenomenon is known as inelastic scattering. When a change in the wavelength of light is greater than $1cm^{-1}$ it is called Raman scattering. If there is no change in wavelength it is called Elastic Scattering. When the incident light is polarized it is used to analyze the molecular structures by Raman peaks [41].

In our research, we focus on G, D, D' and 2D peaks. G peak corresponds to the E_{2g} phonon at the Bernoulli zone center, which is common in sp^2 hybridization. The D peak is formed due to the vibrations of atoms in the material. The surface defects due to impurities result in the D' peak. The 2D peak is the second order of D peak [33].

Figure 11. Raman microscope system with Leica Microscope

Enwave uSense I-785 Raman Microscope System with Leica Microscope; Enwave 785NM Raman System is used for the Raman spectra analysis.

X-ray photoelectron Spectroscopy (XPS)

When X-ray photons are irradiated on a solid surface the core electrons in the surface atoms are emitted with a great amount of kinetic energy (E_k). This is known as the photoelectric effect. To make the electrons leave the surface the energy (E_p) of X-ray photons should be more than the binding energy of electrons and atoms.

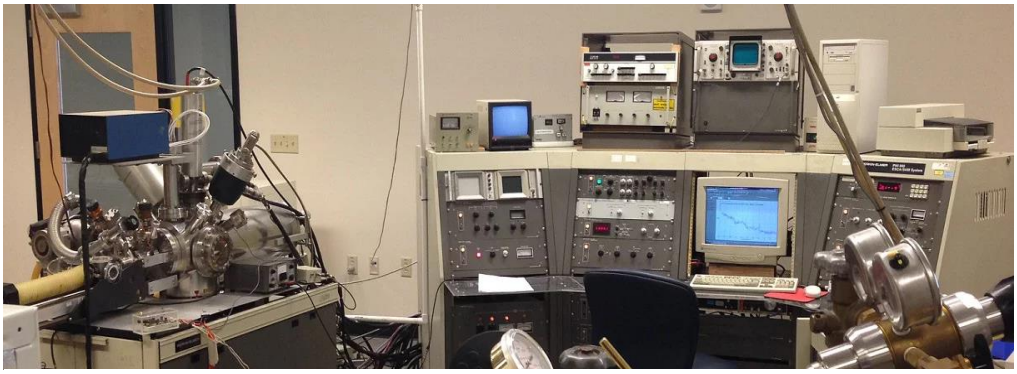

Figure 12. X-ray Photoelectron Microscope

$E_p = E_k + E_B + \phi$

where E_B is the Binding energy of the electron to the nucleus relative to the Fermi level.

E_p is the energy of photon

ϕ is the work function

The binding energy of the electron changes if the atoms are bonded to other chemical groups, as a result, we see the shift in the peaks of Binding energy. This shift will help in determining the chemical composition of the elements on the surface. This also helps in determining different elements present on the surface. Hence we call XPS as

electron spectroscopy of Chemical analysis. In this research, we are trying to find the elements on the surface of the sample and the binding energies of different compounds available on the surface of the sample [43].

X-ray diffraction

X-ray diffraction (XRD) plays a vital role in the fields of metallurgy and material sciences. The crystallinity of the solids is determined by the XRD.

Figure 13. Rigaku Miniflex X-ray equipment

When X-ray photons interact with a surface there will be absorption and scattering of photons takes place. There will be elastic scattering between some phonons and electrons of atomic nuclei. But the crystalline structures are periodic which results in

constructive and destructive scattering, which can be further analyzed to determine the crystal structure of materials. According to Bragg's law in case of constructive interference.

$n\lambda = 2d_{hkl} \sin s\theta$

Where n is the order of diffraction, θ is the angle of diffraction, d is the interatomic spacing between planes and h, k, l are miller indices. [27, 42]

In this research, we use the Rigaku mini flex 600 X-ray system to find the 2θ angles for the Barium titanate sample prepared. Miller indices are calculated for respective peaks and then compared with the standard values to determine the crystallinity of Barium Titanate.

Scanning electron microscopy and electron dispersive X-ray spectroscopy (EDX)

Scanning electron Microscope creates the images of any electrically conductive surface by using a beam of electrons coming from a source.

Figure 14. Scanning electron Microscope

When electrons from the source interact with the electrons on the surface secondary electrons are scattered from the surface. The deflected electrons which are more than 90º angle are called backscattered electrons and be utilized for producing topographical images [42].

Due to the collision of the electron beam with the sample X-rays are emitted. The X-ray spectrum is different for different materials. The Collison of the electron beam with the sample surface creates a hole in the nucleus by ejecting the electron, which also releases the X-ray continuum spectrum. To fill the hole the electron in higher

energy level jumps to that nucleus releasing characteristic X-ray which can be decoded to analyze the elemental composition [42].

In this research, we use the Hitachi VP-SEM S3400N Scanning electron microscope for topographical imaging of samples followed by elemental analysis.

CHAPTER VI: EXPERIMENTAL PROCEDURE

Synthesis of Graphene on Copper (Cu) foil

- Copper samples (Alfa Aesar 0.025 mm, 10950, CAS: 7440-50-8) of dimensions 8 x 8 mm and 10X10 mm size are cut from the sheet of copper foil.
- Samples are sonicated in acetone for 10 min, followed by sonication in alcohol for 10 min.
- Samples are then etched in 16M hydrochloric acid (HCl) for four minutes and then sonicated in alcohol again for 10min.
- Samples are air-dried and placed inside the quartz tube of the split tube furnace.
- At room temperature argon (Ar), hydrogen (H_2) and methane (CH_4) are purged for 10 min Ar at 100 sccm, CH_4 at 50 sccm, H_2 at100 sccm.
- Stop CH4. Flow Ar and H_2 at the same rate for 10 min and then start heating the furnace to 900℃
- Once the temperature reaches 900℃, hold the system at 900℃ for an additional 10 minutes for Reduction of gases in the presence of Hydrogen.
- At 900℃, introduce CH_4 at 50 sccm to synthesize graphene with Ar and hydrogen maintained at earlier rates for 15 minutes.
- After synthesis, the samples are gradually cooled down to 500℃ in the presence of Ar. From 500℃ the samples are cooled down to room temperature rapidly.
- The samples are then characterized using Raman spectroscopy.

  The split tube Furnace with a gas flow regulator used for the synthesis and sintering process is shown in the figure.

Figure 15. Split tube Furnace with Gas flow regulator

Coating and Sintering of Graphene samples

- Various concentrations of barium titanate (Alfa Aesar Barium Titanium Oxide, polymeric precursor, CAS: 12047-27-7) solutions are made by varying the weights of the precursor.
- 0.05 gm and 0.15gm of Barium titanate precursor is ultrasonicated in 15 ml of isopropyl alcohol for 20 minutes separately.
- Now the graphene samples are ultrasonicated in the resultant solution of Barium titanate and isopropyl alcohol for 20 minutes.
- Samples are then air-dried and placed in a crucible and mounted in the furnace for sintering.
- Samples are heated for 2 hours in the presence of Ar at 50 sccm at 700℃ and 900℃. Then the samples are cooled down slowly to 500℃ and then rapidly cooled down to room temperature.
- Now the samples are characterized by using X-ray photon electron spectroscopy, X-ray diffraction, scanning electron microscopy and elemental dispersive X-ray spectroscopy.

Figure 16. Optical image of Barium Titanate sintered samples in the crucible

CHAPTER VII: RESULTS AND DISCUSSION

Raman Spectra Analysis

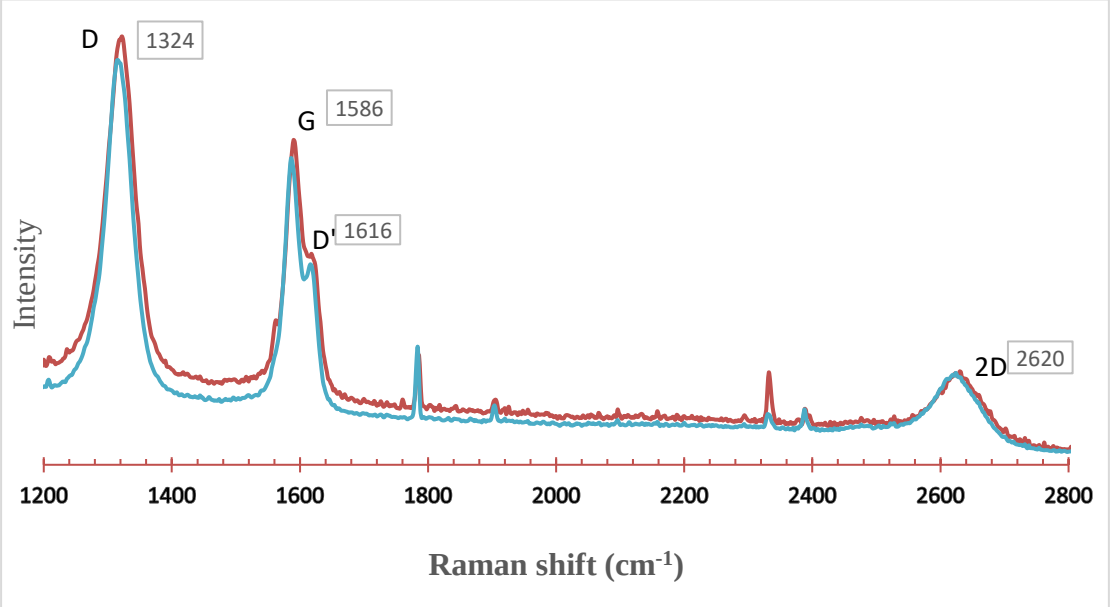

Figure 17. Raman spectroscopy of 15 minitues growth Graphene

Raman spectroscopy of the samples has shown G peak at 1586cm^{-1} D peak at 1324 cm^{-1} and 2D peak at 2620 cm^{-1} and D' is seen at 1616 cm^{-1}. According to Zabel, J et al [33] G peak is seen around 1580 cm^{-1} and D peak due to breathing modules is seen around 1360 cm^{-1} and D' peak determining surface defects are seen around 1620 cm^{-1}. By comparing the results, since the 2D peak is not sharp we conclude that the CVD-growth graphene is few-layer thick and the split of G peak as D' peak tells us that the graphene is defective.

SEM analysis

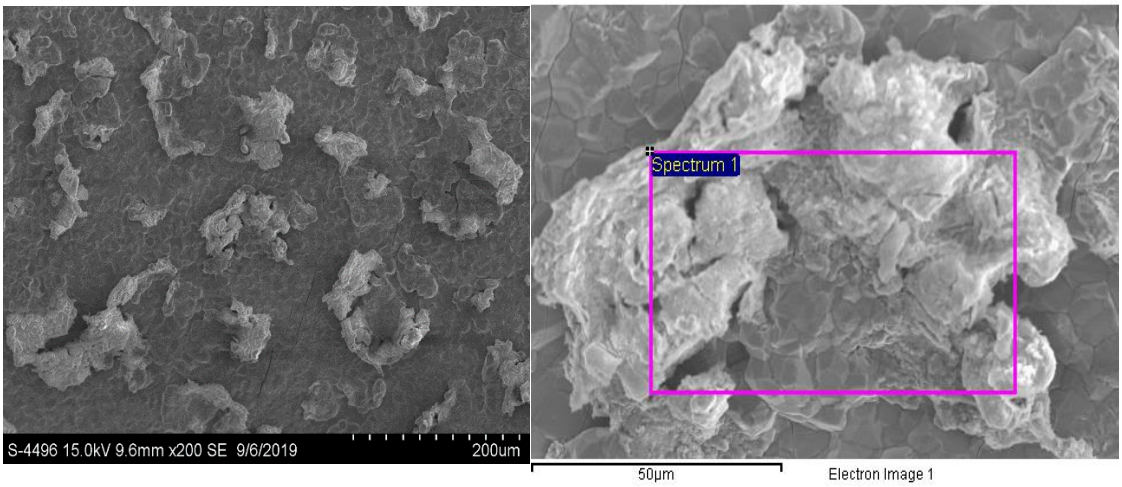

Figure 18. Figure 18. SEM images of Graphene Barium Titanate samples

Scanning electron microscope images show the distribution of Barium titanate of 200µm thick clusters on the graphene-copper template.

EDX Analysis

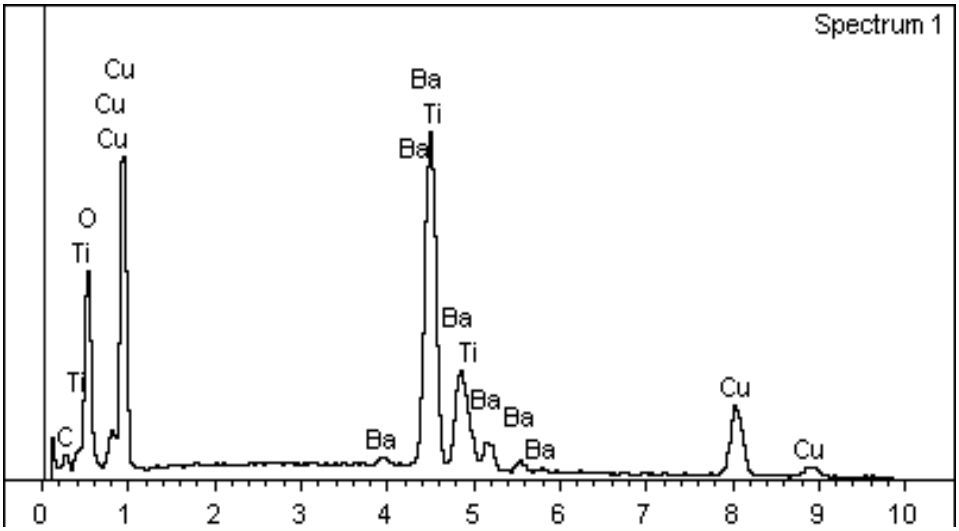

Figure 19. EDX anlaysis of Copper Graphene and Barium Titanate

The above graph of EDX analysis confirms the presence of Carbon, Copper, Titanium Oxygen and Barium in the selected region of the template.

Thermogravimetric analysis

Thermogravimetric analysis was conducted by heating the copper foil sample with graphene. The sample placed in the crucible and heated to 1000℃ in the presence of oxygen for 80 minutes. The weight of the sample decreased by 0.127% showing the yield of Graphene. The weight of the sample before analysis is 13.936 mg. 0.12% of 13.936 mg would be 0.0177mg. So, we conclude that 0.0177 milligrams of Graphene are produced by Chemical Vapor Deposition on copper foil substrate of 8mm x 8mm.

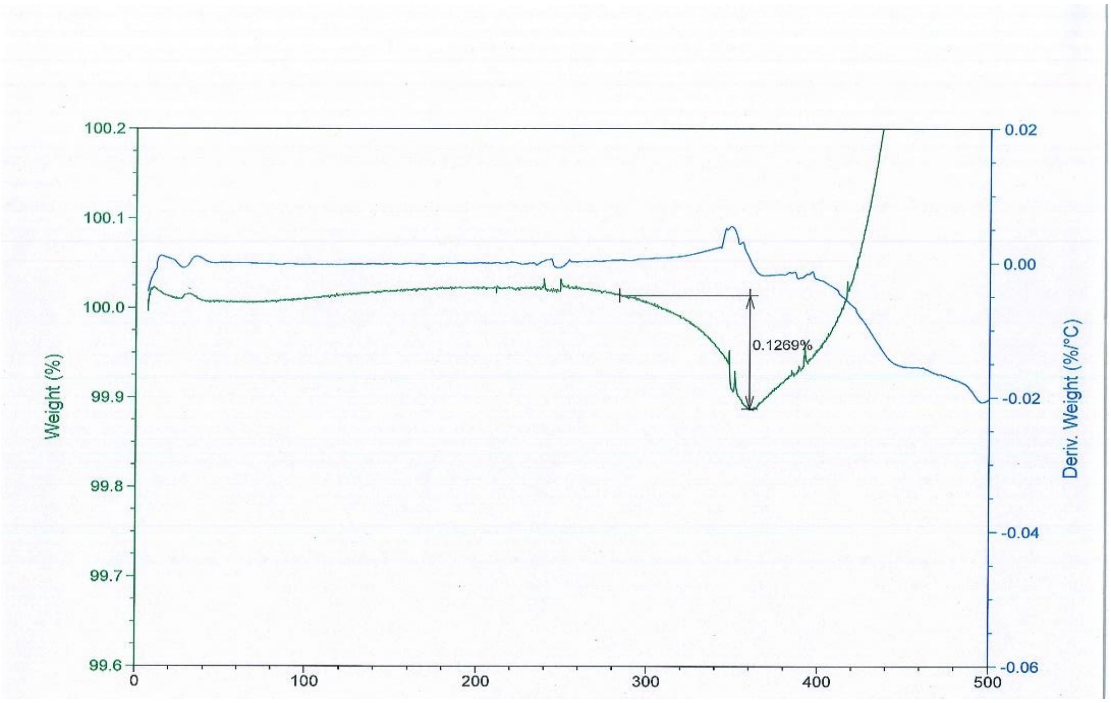

Figure 20. TGA analysis of Graphene

XRD Analysis

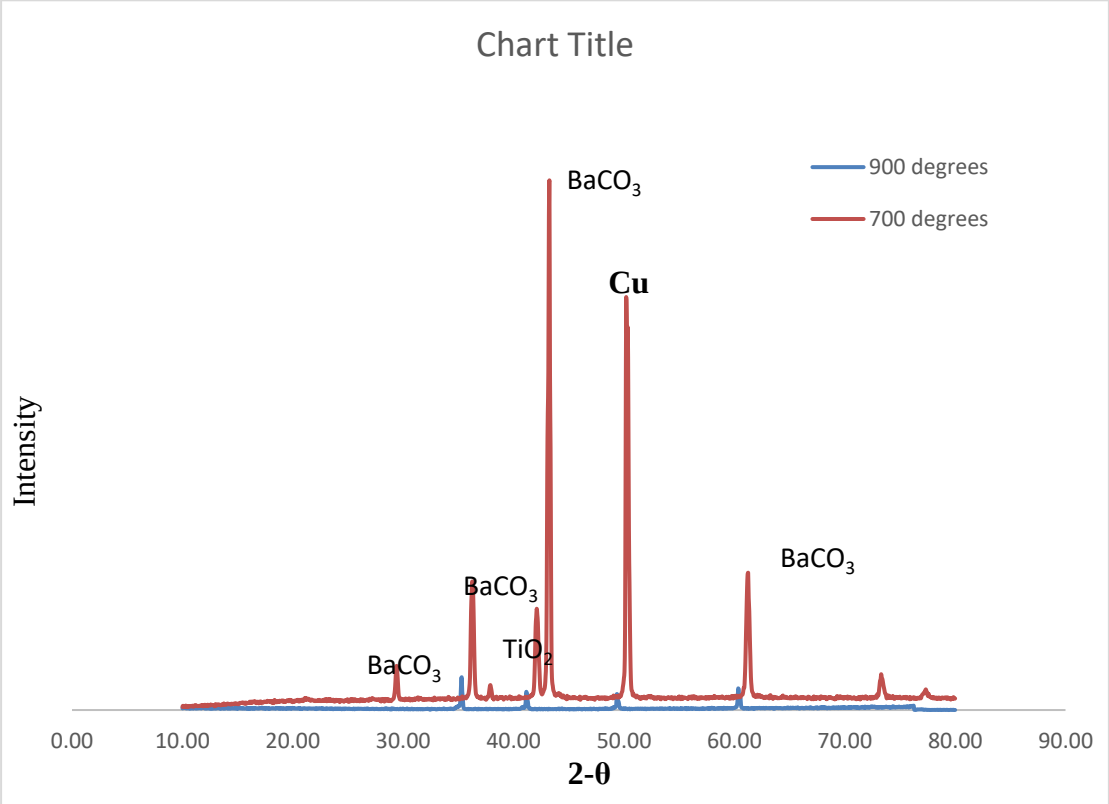

Figure 21. XRD peaks of Barium Titanate

The peaks in the graph are named from the literature. According to Zali et al [40] increasing the temperature of sintering would eliminate the peaks coming from unreacted $BaCO_3$ and Titanium Dioxide. Hence from the results obtained from XRD has shown an increase in the sintering temperature disappeared the sharp peaks coming from Barium carbonate, but the Titanium dioxide peaks are still there at 900℃ temperature. This shows that $BaTiO_3$ is not completely sintered at 2 hours of sintering time and 900℃ of sintering temperature.

XPS Analysis

X-ray photoelectron spectra (XPS) were acquired using a Perkin-Elmer PHI 560 system with a double pass cylindrical mirror analyzer operated using a Mg K∝ anode with a hν = 1253.6 eV photon energy operated at 250 watts and 13 kV. $BaTiO_3$-graphene-Copper sample was mounted onto a custom-built sample holder and inserted into the XPS system via turbo-pumped antechamber. System pressure did not exceed 1 x 10^{-8} torr during scans. The observed C 1s core level at 284.4 eV binding energy (BE) denotes adventitious carbon was used for charge correction. Core level intensities of the C 1s, Ba 3d, Cu 2p, O 1s, Ti 2p orbitals were normalized using their known atomic sensitivity factors. XPS peaks were curve-fitted using 70%-to-30% Gaussian-Lorentzian line shapes with Shirley background subtractions. BE peak envelops were de-convoluted using casaXPS ver. 2.2.107 (Devonshire, UK) software.

Table 2. Atomic percentages and Binding energies of elements in the sample

Orbitals	**Atomic Percentage**	**Binding Energy peaks (Fwhm, % integrated peak area)**
Carbon 1s	9.99%	284.7 eV (2.2, 100%)
Barium 3d	0.17%	779.1 eV (2.4, 54.0%), 794.4 eV (2.7, 46.0%)
Copper 2p	33.5%	931.5 eV (2.0, 37.8%), 951.5 eV (2.3, 19.4%), 963.3 eV (3.5, 3.13%), 942.7 eV (4.2, 9.2%), 953.9 eV (3.5, 8.86%), 961.3 eV (2.4, 2.52%), 933.3 eV (3.0, 19.0%)
Oxygen 1s	56.3%	529.9 eV (2.3, 84.0%), 532.0 eV (2.8, 16.0%)
Titanium 2p	0.033%	456.5 eV (2.7, 100%)

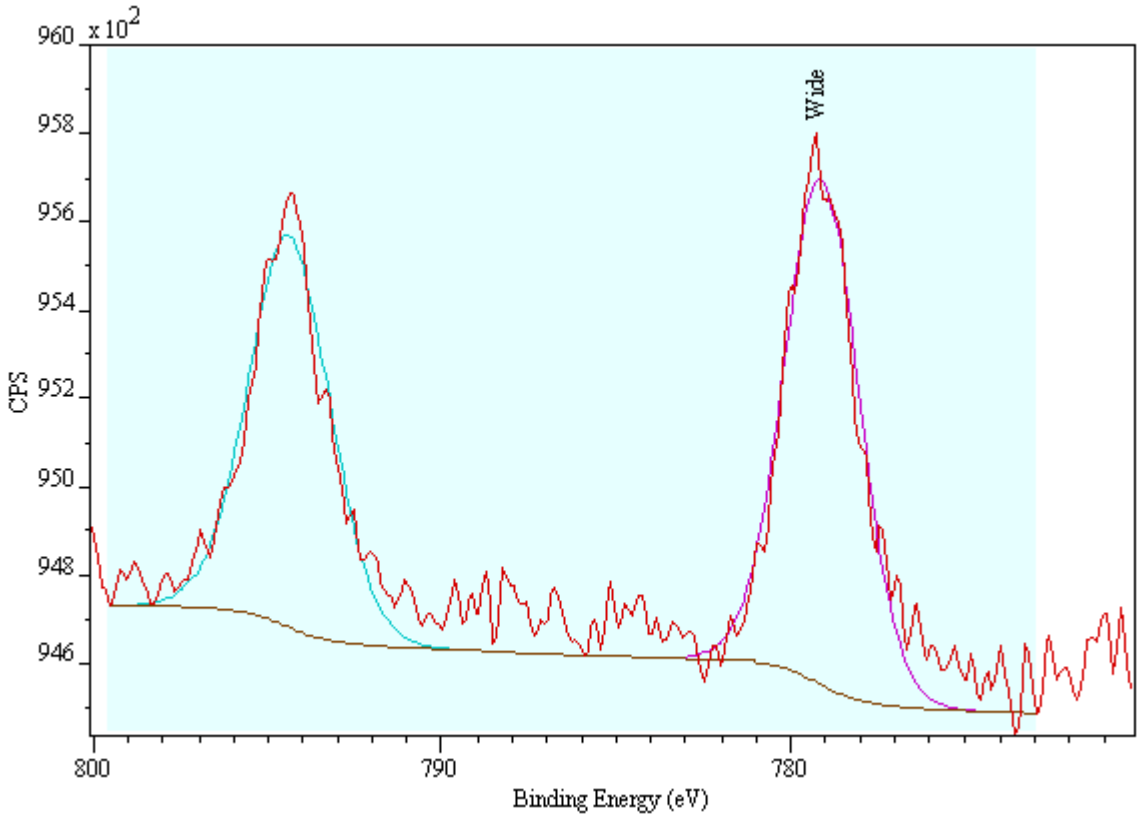

Figure 22. Binding energies of Barium

The peaks at 779.91ev and 794.4ev indicates the nature of bonding of 3d orbital of Barium.

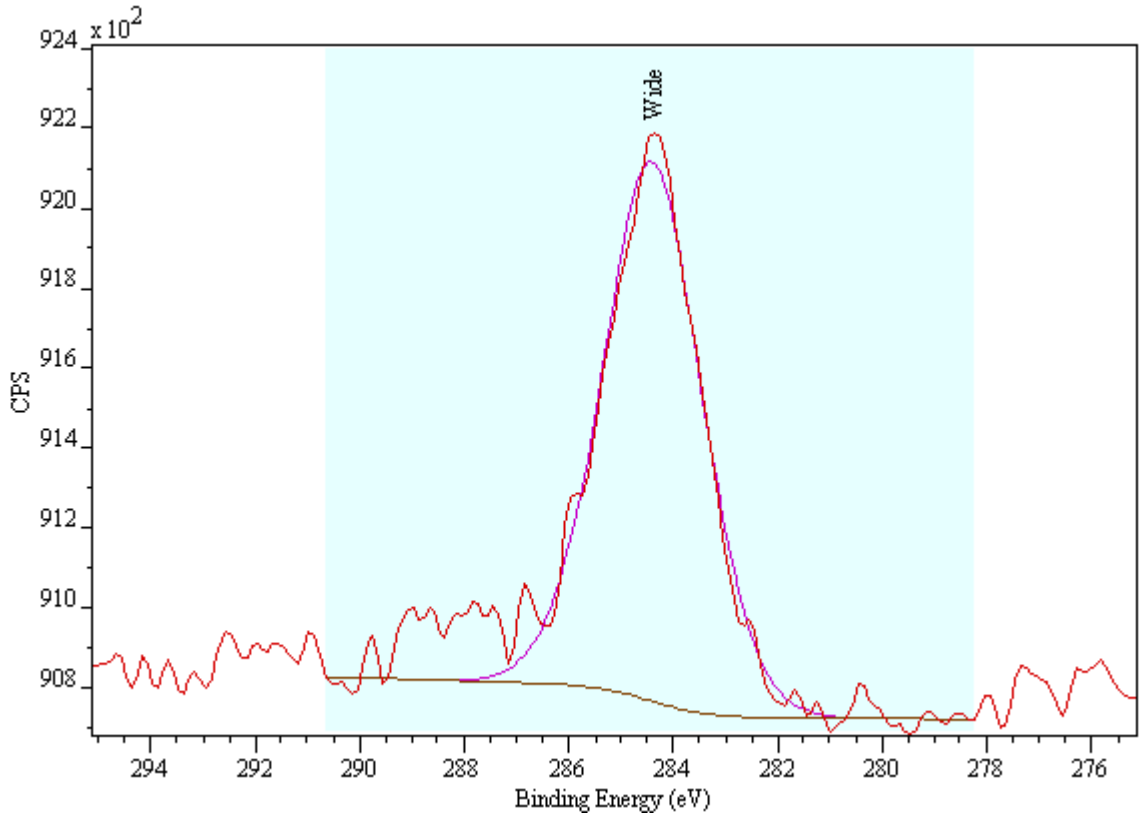

Figure 23. Binding Energies of Carbon 1s orbital

The peak at 284.7ev indicates nature of bonding of 1s orbital of Carbon.

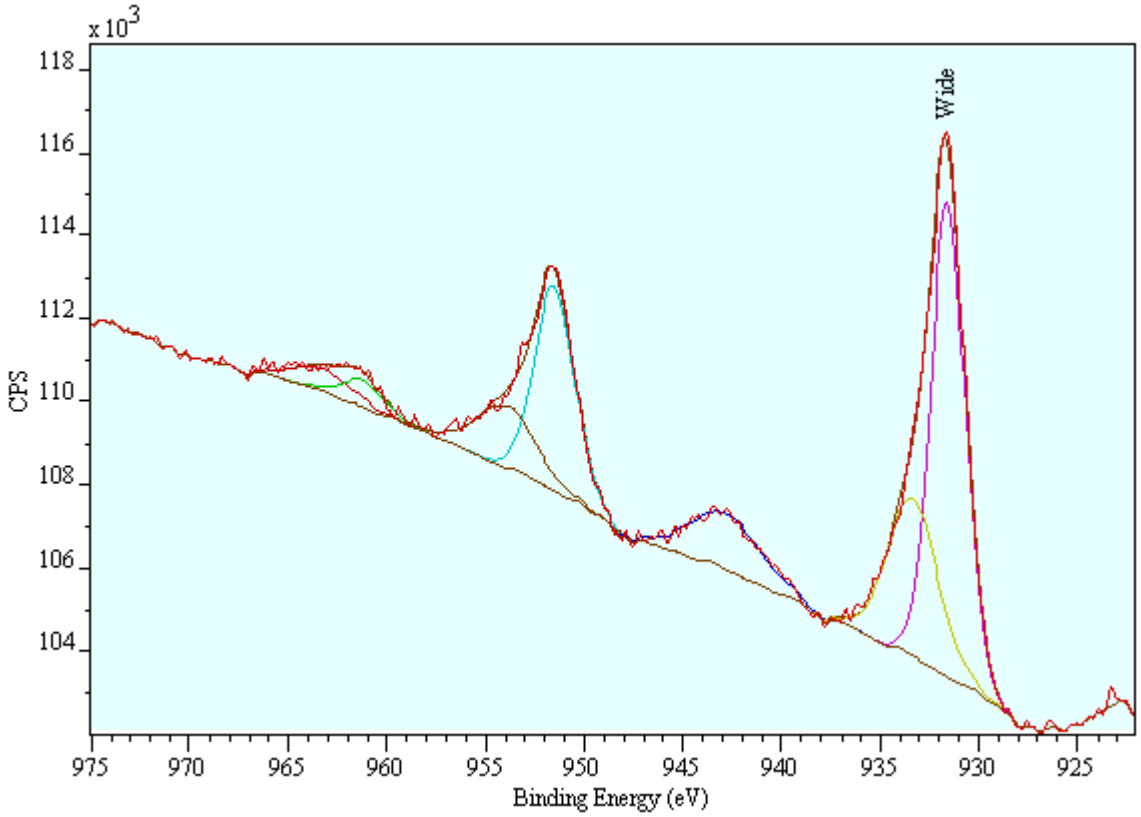

Figure 24.Binding Energies of Copper 2p orbital

Peaks at different binding energies shows the nature of bonding of copper 2p orbital.

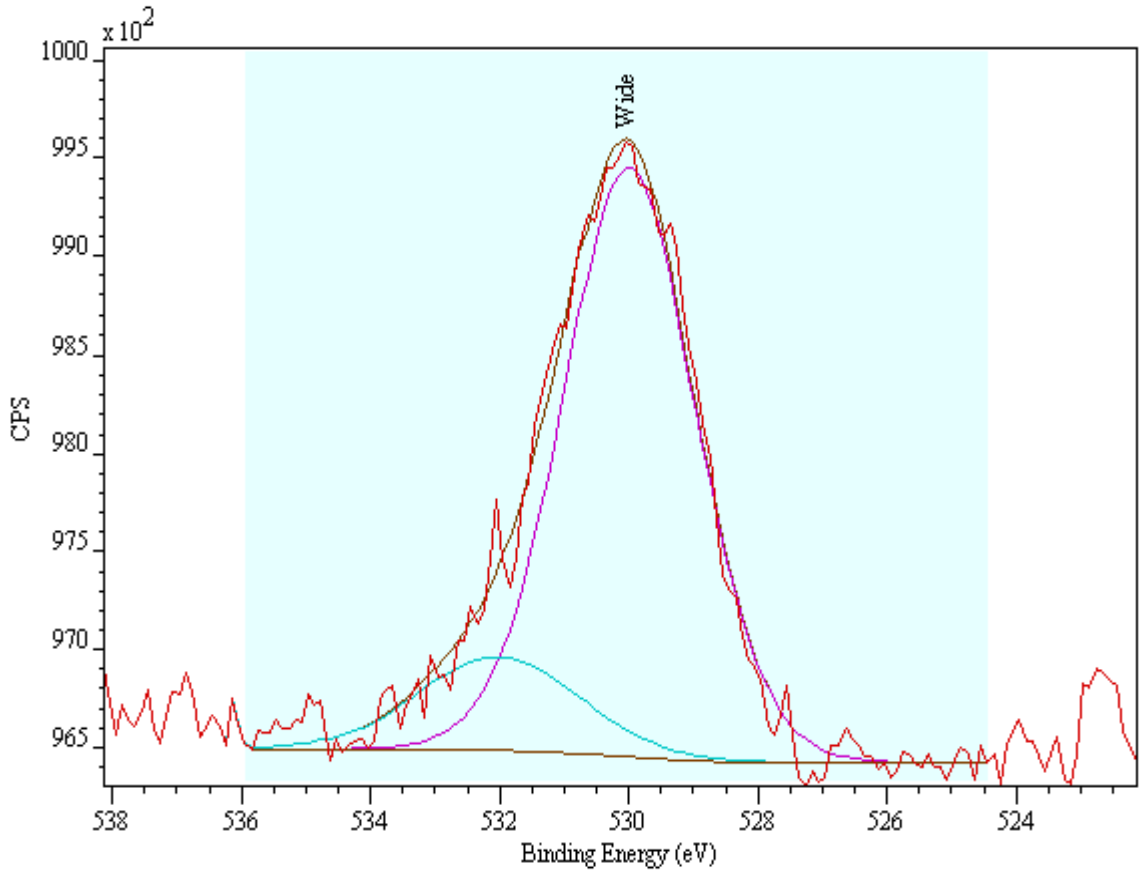

Figure 25. Binding Energy of Oxygen 1s orbital

The peak at 529.9ev and 532.0ev indicates nature of bonding of 1s orbital of oxygen.

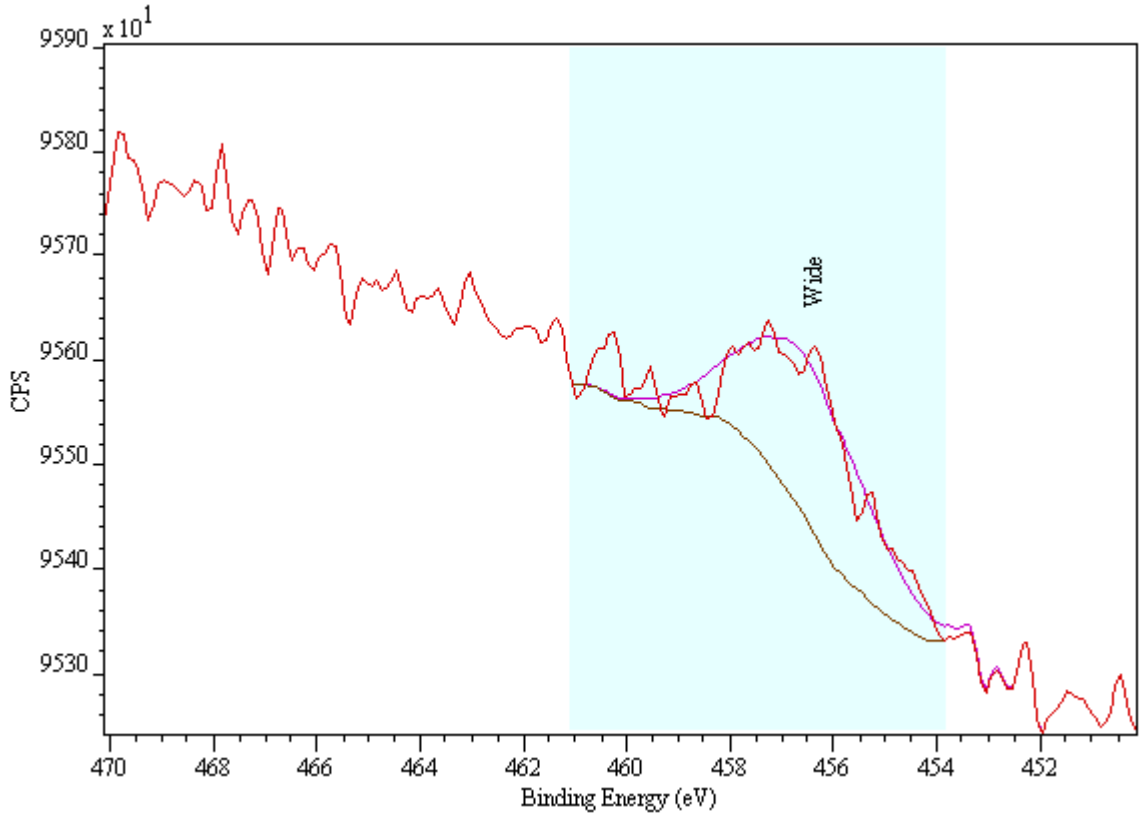

Figure 26. Binding Energy of Titanium 2p orbital

The peak at 456.5ev indicates nature of bonding of 2P orbital of Titanium.

Hence comparing the results with the literature Vishwas et al [23], the peaks at binding energy 529.9ev and 532.0ev indicate the nature of bonding of oxygen 1s orbital with different elements present in the sample. The peak at 532.0ev corresponds to the copper oxides in the sample and the peak at 529.9ev corresponds to the barium-titanium-oxygen bonding. The Ba 3d and that the Ti 2p are consistent with the core level shifts for $BaTiO_3$.

CHAPTER VIII: CONCLUSION

Raman spectroscopy after CVD has confirmed the presence of a few-layer graphene on the copper template. After the sintering of barium titanate, EDX analysis has confirmed the presence of all the elements barium, titanium, oxygen and carbon, that are synthesized. XPS has confirmed the barium titanium and oxygen bonding uniformly present all over the sample. Hence we can conclude that using the ultrasonication technique we have successfully coated few layer CVD-graphene with piezoelectric ceramic $BaTiO_3$.

CHAPTER IX: FUTURE WORK

$BaTiO_3$ has to be sintered at different temperatures for different sintering times and characterized to find the optimal temperature that makes $BaTiO_3$ reach its actual crystalline structure. Just like ultrasonication, several cost-effective coating techniques are available in the industries. They are sol-gel, physical vapor coating, spin coating, sputter coating, electrochemical coating, and chemical vapor deposition, etc., graphene can be tested coating with each of those techniques and then characterized. Some of the techniques might be cost-effective but the quality of the compound might be ineffective. Depending on the necessity of application different coating techniques have to be adapted and then characterized. After the coating techniques are optimized the samples need to be electrically polarized using an electronic polarizer and tested for piezoelectric properties. These samples can be fabricated as a small cantilever beam and can be used as MEMS.

REFERENCES

1. Novoselov, K. S., Jiang, D., Booth, T., Khotkevich, V. V., Morozov, S. M., & Geim, A. K. (2005). Two dimensional atomic crystals. https://doi.org/10.1073/pnas.0502848102.
2. K. S. Novoselov, A. K. Geim, S. V. Morozov, D. Jiang, Y. Zhang, S. V. Dubonos, … A. A. Firsov. (2004). Electric field effect in atomically thin carbon films. *Science, 306(5696), 666. Retrieved from* http://search.ebscohost.com/login.aspx?direct=true&db=edsjsr&AN=edsjsr.3839379&site=eds-live&scope=site
3. Castro, E. V., Novoselov, K. S., Morozov, S. V., Peres, N. M. R., Santos, J. M. B. L. dos, Nilsson, J., … Neto, A. H. C. (2008). Electronic properties of a biased graphene bilayer. https://doi.org/10.1088/0953-8984/22/17/175503
4. Sánchez, C. C. (1), Wåhlander, M. (1), Karlsson, M. (1), Quintero, D. C. M. (1), Malmström, E. (1), Nilsson, F. (1), & Hillborg, H. (2). (n.d.). Characterization of reduced and surface-modified graphene oxide in poly(ethylene-co-butyl acrylate) composites for electrical applications. *Polymers, 11(4).* https://doi.org/10.3390/polym11040740
5. Zhang, L., Zhang, F., Yang, X., Long, G., Wu, Y., & Zhang, T. et al. (2013). Porous 3D graphene-based bulk materials with exceptional high surface area and excellent conductivity for supercapacitors. *Scientific reports, 3(1).* doi: 10.1038/srep01408
6. Wang, L., Yin, M., Zhong, B., Jaroszynski, J., Mbamalu, G., & Datta, T. datta@mailbox. sc. ed. (2019). Quantum transport properties of monolayer graphene with antidot lattice. *Journal of Applied Physics, 126(8), N.PAG.* https://doi.org/10.1063/1.5100813

7. Wu, Y., Zhang, X., Jie, J., Xie, C., Zhang, X., & Sun, B. et al. (2013). Graphene transparent conductive electrodes for highly efficient silicon nanostructures-based hybrid heterojunction solar cells. *The Journal of Physical Chemistry C, 117(23), 11968-11976.* doi: https://doi.org/10.1021/jp402529c
8. Babichev, A. V. (1,2,3,5), Egorov, A. Y. (1), Vitusevich, S. (2), Tchernycheva, M. (3), & Gasumyants, V. E. (4). (n.d.). Contact properties to cvd-graphene on gaas substrates for optoelectronic applications. *Nanotechnology, 25(33).* https://doi.org/10.1088/0957-4484/25/33/335707
9. Dong Soo Choi, Seung Ho Han, Hyeongkeun Kim, So Hee Kang, Yena Kim, Cheol-Min Yang, … Woo Seok Yang. (2014). Flexible electrochromic films based on cvd-graphene electrodes. *Nanotechnology, 25(39), 1*. https://doi.org/10.1088/0957-4484/25/39/395702
10. Lee, S.-K., Rana, K., & Ahn, J.-H. (n.d.). Graphene films for flexible organic and energy storage devices. *Journal of physical chemistry letters, 4(5), 831–841.* https://doi.org/10.1021/jz400005k
11. Huang, L., Wang, Z., Pu, J., Shen, L., & Zhang, J. (2013). Graphene pattern by gravure printing for wireless strain sensor. *2013 seventh international conference on sensing technology (icst).* doi: 10.1109/icsenst.2013.6727681
12. Zhou, S., Zhuo, C., Min, Q., & Li, E. (2017). Graphene based thermoelectric energy harvesting in 3d ics. *2017 IEEE electrical design of advanced packaging and systems symposium (edaps).* doi: 10.1109/edaps.2017.8276959
13. Ciminelli, C., DellrOlio, F., Brunetti, G., Conteduca, D., & Armenise, M. (2018). Graphene/silicon schottky junction solar cells. *2018 20th international conference on transparent optical networks (icton).* doi: 10.1109/icton.2018.8473835

14. Graphenea. (2019). High quality graphene producer. [online] Available at: https://www.graphenea.com/ [Accessed 5 Nov. 2019]
15. Haydale. (2019). Haydale | creating material change. [online] Available at: https://haydale.com/ [Accessed 5 Nov. 2019].
16. Talgaresources.com. (2019). Talga resources. [online] Available at: http://www.talgaresources.com/irm/content/default.aspx [Accessed 7 Nov. 2019].
17. Singh, M., Yadav, B., Ranjan, A., Kaur, M., & Gupta, S. (2017). Synthesis and characterization of perovskite barium titanate thin film and its application as lpg sensor. *Sensors and actuators b: chemical, 241, 1170-1178.* doi: 10.1016/j.snb.2016.10.018
18. Jelena Vukmirović, Djordjije Tripković, Branimir Bajac, Sanja Kojić, Goran M. Stojanović, & Vladimir V. Srdić. (2015). Comparison of barium titanate thin films prepared by inkjet printing and spin coating. *Processing and application of ceramics, (3), 151.* https://doi.org/10.2298/PAC1503151V
19. Hu, S., Luo, C., Li, P. lipengwei@tyut. edu. cnlpw181920@163. co., Hu, J., Li, G., Jiang, H., & Zhang, W. (2017). Effect of sintered temperature on structural and piezoelectric properties of barium titanate ceramic prepared by nano-scale precursors. *Journal of materials science: materials in electronics, 28(13), 9322–9327.* https://doi.org/10.1007/s10854-017-6670-7
20. Zarkoob, H., Ziaei-Rad, S., Fathi, M., & Dadkhah, H. (2012). Synthesis, characterization and bioactivity evaluation of porous barium titanate with nanostructured hydroxyapatite coating for biomedical application. *Advanced engineering materials, 14(6), b322.* Retrieved from http://search.ebscohost.com/login.aspx?direct=true&db=edb&AN=76349485&site=eds-live&scope=site

21. Berger, C., Song, Z., Li, T., Li, X., Ogbazghi, A. Y., Feng, R., … de Heer, W. A. (2004). Ultrathin epitaxial graphite: 2d electron gas properties and a route toward graphene-based nanoelectronics. https://doi.org/10.1021/jp040650f

22. Sahoo, S. K., & Mallik, A. (n.d.). Synthesis and characterization of conductive few layered graphene nanosheets using an anionic electrochemical intercalation and exfoliation technique. *Journal of materials chemistry c, 3(41), 10870–10878.* https://doi.org/10.1039/c5tc01893e

23. S. Moshgi Asl, A. Afshar, & Y. Yaghoubinezhad. (2018). An electrochemical synthesis of reduced graphene oxide/zinc nanocomposite coating through pulse-potential electrodeposition technique and the consequent corrosion resistance. *International journal of corrosion.* https://doi.org/10.1155/2018/3028693

24. Huang, Wei-Hao, Cheng-Hsuan Lin, Ben-Son Lin, and Chia-Liang Sun. 2019. "Low-temperature cvd graphene nanostructures on cu and their corrosion properties." *Materials 11 (10). Accessed october 30.* doi:10.3390/ma11101989.

25. Dagher, R. (1), Matta, S. (1), Nguyen, L. (1), Portail, M. (1), Brault, J. (1), Cordier, Y. (1), … Tanaka, S. (4). (n.d.). High temperature annealing and CVD growth of few-layer graphene on bulk AlN and AlN templates. *Physica Status Solidi (A) Applications and Materials Science, 214(4).* https://doi.org/10.1002/pssa.201600436

26. Kim, J., Sakakita, H., & Itagaki, H. (n.d.). Low-temperature graphene growth by forced convection of plasma-excited radicals. *Nano letters.* https://doi.org/10.1021/acs.nanolett.8b03769

27. Kalita, G., Wakita, K., Umeno, M., Hayashi, Y., & Tanemura, M. (2013). Synthesis of continuous graphene on metal foil for flexible transparent electrode

application. *2013 ieee 5th international nanoelectronics conference (inec).* doi: 10.1109/inec.2013.6466023

28. Juang, Z.-Y., Wu, C.-Y., Lu, A.-Y., Su, C.-Y., Leou, K.-C., Chen, F.-R., & Tsai, C.-H. (2010). Graphene synthesis by chemical vapor deposition and transfer by a roll-to-roll process. Retrieved from http://search.ebscohost.com/login.aspx?direct=true&db=edsarx&AN=edsarx.1005.1510&site=eds-live&scope=site
29. Lee, J., Seo, J., Jung, S., Park, K., & Park, H. (2018). Unveiling the direct correlation between the cvd-grown graphene and the growth template. *Journal of nanomaterials, 1–6.* https://doi.org/10.1155/2018/7610409
30. Xuesong Li, Weiwei Cai, Jinho An, Seyoung Kim, Junghyo Nah, Dongxing Yang, … Rodney S. Ruoff. (2009). Large-area synthesis of high-quality and uniform graphene films on copper foils. *Science, 324(5932), 1312.* https://doi.org/10.1126/science.1171245
31. ALYÖRÜK, M. M. (2016). The effect of triangular cavities on piezoelectric property of graphene. *Anadolu university of sciences & technology - a: applied sciences & engineering, 17(3), 585–593.* https://doi.org/10.18038/btda.47955
32. Brazhe, R. A., Kochaev, A. I., & Sovetkin, A. A. (2013). Piezoelectric effect in graphene-like 2D supracrystals with a periodic perforation breaking the central symmetry. *Physics of the solid state, 55(9), 1925–1928.* https://doi.org/10.1134/S1063783413090060
33. Zabel, J., Nair, R. R., Ott, A., Georgiou, T., Geim, A. K., Novoselov, K. S., & Casiraghi, C. (2012). Raman spectroscopy of graphene and bilayer under biaxial strain: bubbles and balloons. https://doi.org/10.1021/nl203359n

34. Kumazawa, H., & Masuda, K. (1999). Fabrication of barium titanate thin films with a high dielectric constant by a sol–gel technique. *Thin Solid Films, 353(1), 144–148.* https://doi.org/10.1016/S0040-6090(99)00427-7

35. Bedekar, V., Singh, G., Mahajan, R. L., & Priya, S. (2009). Synthesis and microstructural characterization of barium titanate nanoparticles decorated sicn-mwcnt nanotubes - "nanonecklace." *Ferroelectrics letters section, 36(5–6), 133–140.* https://doi.org/10.1080/07315170903446553

36. Bedekar, V., Murayama, M., & Mahajan, R. L. (2010). Controlled Synthesis of BaTiO3-Coated Multiwall Carbon Nanotubes. *Journal of the American ceramic society, 93(11), 3618–3623.* https://doi.org/10.1111/j.1551-2916.2010.04154.x

37. Zali, N., Mahmood, C., Mohamad, S., Foo, C., & Murshidi, J. (2014). X-ray diffraction study of crystalline barium titanate ceramics. doi: 10.1063/1.4866124

38. Kumar, A. (2013). Graphene decorated substrates and their interfacial characteristics (3613168). *Available from ProQuest Dissertations & Theses Global. (1511024080). Retrieved from* https://ezproxy.mtsu.edu/login?url=https://search.proquest.com/docview/1511024080?accountid=4886

39. Stankovich, S., Dikin, D. A., Piner, R. D., Kohlhaas, K. A., Kleinhammes, A., Jia, Y., … Ruoff, R. S. (2007). Synthesis of graphene-based nanosheets via chemical reduction of exfoliated graphite oxide. *Carbon, 45(7), 1558–1565.* https://doi.org/10.1016/j.carbon.2007.02.034

40. Powell, M. (2017). Chemical vapor deposition (CVD) [electronic resource] : types, uses, and selected research. *Nova Science Publishers, Inc.* Retrieved from http://search.ebscohost.com/login.aspx?direct=true&db=cat00263a&AN=mts.b3704376&site=eds-live&scope=site

41. Zhang, S.-L. (2012). Raman spectroscopy and its application in nanostructures. [electronic resource]. *John Wiley & Sons.* Retrieved from http://search.ebscohost.com/login.aspx?direct=true&db=cat00263a&AN=mts.b2167300&site=eds-live&scope=site

42. Hübschen, G., Altpeter, I., Tschuncky, R., & Herrmann, H.-G. (2016). Materials characterization using nondestructive evaluation methods. *Woodhead Publishing, an imprint of Elsevier.* Retrieved from http://search.ebscohost.com/login.aspx?direct=true&db=cat00263a&AN=mts.b3741796&site=eds-live&scope=site

43. Wagner, J. M. (2011). X-ray Photoelectron Spectroscopy. *New York: Nova Science Publishers, Inc.* Retrieved from http://search.ebscohost.com.ezproxy.mtsu.edu/login.aspx?direct=true&db=e000xna&AN=421872&site=ehost-live&scope=site